Phenylalanine and Tryptophan Scanning Mutagenesis of CYP3A4 Substrate Recognition Site Residues and Effect on Substrate Oxidation and Cooperativity†

Tammy L. Domanski,*,‡ You-Ai He,‡ Kishore K. Khan, Fabienne Roussel, Qinmi Wang, and James R. Halpert

Department of Pharmacology and Toxicology, University of Texas Medical Branch, 301 University Boulevard, Galveston, Texas 77555-1031

Received April 13, 2001

ABSTRACT: Phenylalanine and/or tryptophan scanning mutagenesis was performed at 15 sites within CYP3A4 proposed to be involved in substrate specificity or cooperativity. The sites were chosen on the basis of previous studies or from a comparison with the structure of $P450_{eryF}$ containing two molecules of androstenedione. The function of the 25 mutants was assessed in a reconstituted system using progesterone, testosterone, 7-benzyloxy-4-(trifluoromethyl)coumarin (7-BFC), and α-naphthoflavone (ANF) as substrates. CYP3A4 wild type displayed sigmoidal kinetics of ANF 5,6-oxide formation and 7-BFC debenzylation. Analysis of 12 mutants with significant steroid hydroxylase activity showed a lack of positive correlation between ANF oxidation and stimulation of progesterone 6β-hydroxylation by ANF, indicating that ANF binds at two sites within CYP3A4. 7-BFC debenzylation was stimulated by progesterone and ANF, and 7-BFC did not inhibit testosterone or progesterone 6β-hydroxylation. Correlational analysis showed no relationship between 7-BFC debenzylation and either progesterone or testosterone 6β-hydroxylation. These data are difficult to explain with a two-site model of CYP3A4 but suggest that three subpockets exist within the active site. Interestingly, classification of the mutants according to their ability to oxidize the four substrates utilized in this study suggested that substrates do bind at preferred locations in the CYP3A4 binding pocket.

Cytochrome P450 (CYP)[1] 3A4 is the major drug-metabolizing enzyme in the human liver, oxidizing approximately 50% of drugs currently on the market (*1*, *2*). Consequently, CYP3A4 inhibition or induction is also a major concern in the development of new drugs, as the enzyme is involved in many drug−drug interactions (*3*, *4*). These interactions can be unpredictable, especially in light of the atypical kinetic behavior of CYP3A4 observed in vitro with some substrates such as aflatoxin B_1 (*5*), amitriptyline (*6*), caffeine (*7*), carbamazepine (*8*), progesterone (*9*), and diazepam (*10*, *11*). Such substrates yield sigmoidal v vs S plots, indicative of positive homotropic cooperativity. In addition, effectors such as α-naphthoflavone (ANF) (*9*, *12*) and testosterone (*8*) cause stimulation of CYP3A4 activity toward some substrates, referred to as heterotropic cooperativity. This phenomenon was first noted in vitro with flavonoids (*13*), which were also shown to activate drug metabolism in vivo in a rat model (*14*, *15*). Recently, the CYP3A4-catalyzed formation of 5-hydroxydiclofenac in incubations with human liver microsomes was reported to be stimulated by the presence of quinidine (*16*). In vivo studies with monkeys also demonstrated stimulation of diclofenac metabolism in the presence of quinidine (*17*).

The emerging hypotheses of the mechanism of CYP3A4 cooperativity involve double occupancy of the binding pocket (*6*, *11*, *12*, *18*), triple occupancy of the pocket (*18*−*20*), or the existence of functionally distinct conformers (*21*). Korzekwa et al. described a two-site enzyme model that may account for the atypical enzyme kinetics exhibited by a number of P450 isoforms (*22*). The authors proposed that within a two-substrate-bound active site, both substrates, through rotation and translation within the time frame of the oxidation step, have access to the reactive oxygen but no preferred orientations (*22*). Shou envisioned that there are two distinct substrate binding sites, with each substrate having a preferred orientation (*11*). Our laboratory suggested that the substrate and effector occupy separate positions and that only the former has access to the reactive oxygen (*12*). These models have been used successfully to explain several recent examples of heterotropic cooperativity or lack of competition between two substrates that exhibit Michaelis−Menten kinetics (*23*−*25*).

It is more difficult, however, to utilize two-site models to explain the lack of mutual competitive inhibition observed between certain substrates that exhibit sigmoidal steady-state kinetics or binding isotherms, such as diazepam and testosterone (*26*) or ANF and aflatoxin B_1 (*6*). We therefore

† Supported by Grant GM54995 (J.R.H.) and Center Grant ES06676 from the National Institutes of Health.

* To whom correspondence should be addressed. Telephone: (409) 772-9677. Fax: (409) 772-9642. E-mail: tadomans@UTMB.edu.

‡ These authors contributed equally to the work presented in this paper.

[1] Abbreviations: CYP, cytochrome P450; ALA, δ-aminolevulinic acid; ANF, α-naphthoflavone; 7-BFC, 7-benzyloxy-4-(trifluoromethyl)-coumarin; CHAPS, 3-[(3-cholamidopropyl)dimethylammonio]propanesulfonate; DOPC, dioleoylphosphatidylcholine; HEPES, *N*-(2-hydroxyethyl)piperazine-*N*′-2-ethanesulfonic acid; 7-HFC, 7-hydroxy-4-(trifluoromethyl)coumarin; IPTG, isopropyl β-D-thiogalactoside; MOPS, 4-morpholinepropanesulfonic acid; OH, hydroxy; PCR, polymerase chain reaction; RPR 106541, (20*R*)-16α,17α-[butylidenebis(oxy)]-6α,9α-difluoro-11β-hydroxy-17β-(methylthio)androst-4-en-3-one.

10.1021/bi010758a CCC: $20.00 © 2001 American Chemical Society
Published on Web 08/04/2001

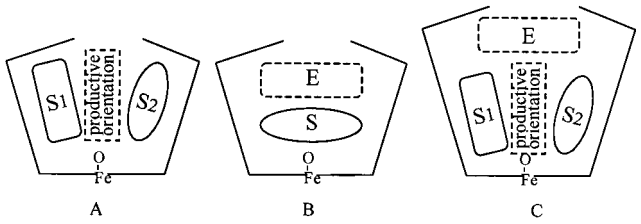

FIGURE 1: Working models of the active site of CYP3A4. The binding pocket is schematically represented by the outer solid black lines, and the heme is indicated by the horizontal portion including the iron (Fe). E represents a noncatalytic effector site; S, S_1, and S_2 represent substrate binding sites.

recently proposed a model in which each substrate occupies a preferred location in the vicinity of the active oxygen and where the substrates compete for a more distal effector site (*19*) (Figure 1C). A critical distinction between models involving double or triple occupancy of the binding pocket is whether effectors such as ANF bind at the same location when serving as activators as when serving as substrates. A key observation of Korzekwa et al. (*22*) was that phenanthrene and ANF showed binding constants as effectors similar to their respective K_m values as substrates. However, more recently that same group reported a much higher K_m value for ANF oxidation by CYP3A4 (*23*). Furthermore, with purified recombinant CYP3A4, sigmoidal steady-state kinetics of ANF oxidation (*20*) and sigmoidal binding curves (*19*, *20*) have been reported. Therefore, the possibility that CYP3A4 has a separate noncatalytic effector site (Figure 1B,C) remains a strong one and has a precedent in bacterial $P450_{eryF}$. That enzyme exhibits cooperative binding of androstenedione, and recent X-ray crystallographic analysis revealed two molecules of steroid in the active site, one of which appears to be located too far from the heme to have access to the active oxygen (*27*).

Whereas other laboratories have utilized a variety of substrates, effectors, and inhibitors as mechanistic probes of CYP3A4 (*6*, *11*, *18*, *20*, *22*−*25*), our approach has been to perturb the enzyme by site-directed mutagenesis. Previous work in our laboratory has implicated a number of CYP3A4 amino acid residues in substrate recognition (*28*−*33*). In those studies substitutions were made with side chains of similar or smaller size, and most of the residues identified (119, 301, 304, 305, 309, 369, 370, 373, 479) have direct active site counterparts in the subsequently determined X-ray crystal structure of mammalian CYP2C5 (*34*, *35*). Other studies utilized similar methods to generate larger side chains at residues Leu-211 and Asp-214, and the results implicated these sites in both heterotropic and homotropic cooperativity (*12*). Analysis of Ala and Trp mutants of CYP3A4 residue Phe-304 indicated that this amino acid plays a dual role, contributing to substrate oxidation and effector action (*19*, *28*). Interestingly, residues 211, 214, and 304 in CYP3A4 appear to map to residues in $P450_{eryF}$ that are within 5 Å of the more distal androstenedione (*27*).

In the present investigation 15 amino acid residues in CYP3A4 suggested by analogy with CYP2C5 or $P450_{eryF}$ were substituted with the largest nonpolar amino acids, Phe and/or Trp, and function was assessed with four substrates that yield sigmoidal steady-state kinetics with wild-type CYP3A4. The goals were to (1) identify additional residues that contribute to cooperativity, (2) assess the relationship between the substrate and effector properties of ANF, and (3) seek evidence for preferred locations within the active site for oxidation of the different substrates. The results of functional and correlational analyses and molecular modeling provide further evidence to support a three-site model for CYP3A4.

EXPERIMENTAL PROCEDURES

Materials. Oligonucleotide primers were obtained from the University of Texas Medical Branch Molecular Biology Core Laboratory (Galveston, TX) or from Sigma Genosys (Woodlands, TX). Restriction enzymes were purchased from Life Technologies, Inc. (Grand Island, NY). The Expand PCR kit and Rapid Ligation kits were obtained from Roche (Indianapolis, IN). The TA cloning kit was obtained from Stratagene (La Jolla, CA). CHAPS, NADPH, DOPC, ANF, ALA, IPTG, progesterone, and testosterone were obtained from Sigma Chemical Co. (St. Louis, MO). The BCA Protein Assay kit was purchased from Pierce (Rockford, IL). [^{14}C]-Progesterone was purchased from DuPont-New England Nuclear (Boston, MA), and [^{14}C]testosterone was purchased from Amersham Pharmacia (Arlington Heights, IL). 7-BFC was purchased from Gentest (Woburn, MA). 7-HFC was purchased from Molecular Probes (Eugene, OR). HEPES was purchased from Calbiochem (La Jolla, CA), and thin-layer chromatography plates [silica gel, 250 μm, Si 250 PA (19C)] were obtained from Baker (Phillipsburg, NJ). Talon metal affinity resin was purchased from Clontech (Palo Alto, CA). All other reagents and supplies were obtained from standard sources.

Construction of Mutant Plasmids. All mutants generated in this study were verified by sequencing to ensure the presence of the desired changes and the absence of extraneous mutations (Protein Chemistry Laboratory, University of Texas Medical Branch, Galveston, TX). Mutants L210W, F213W, I301F/W, and L373F/W were produced using a one-step PCR method. Each mutagenic primer (Figure 2) containing the recognition site for a unique restriction endonuclease was utilized with a vector-specific primer containing a second unique restriction endonuclease recognition site in amplification reactions. The products were cloned directly into pCRII, the presence of the appropriate DNA insert was verified by sequencing, and the appropriate restriction endonucleases were utilized to generate the desired fragments. These fragments were purified with a GeneClean Kit (Bio101, Vista, CA) and ligated into plasmid pKK3A4His or pSE3A4His treated similarly.

Mutants I369F/W and A370F/W were constructed in a similar manner, except plasmids pKK3A4I369VHis and pKK3A4A370VHis, respectively, were used as templates. Four histidine residues were added to the C-terminus of 3A4I369V and 3A4A370V (*30*) as described (*28*). The products of the one-step PCR were treated as described for those above, and the desired restriction fragments were subcloned into pKK3A4I369VHis and pKK3A4A370VHis, respectively.

Mutants F215W, Y307W, and T309F/W were constructed utilizing the Expand PCR kit as described previously (*36*). Plasmid pSE3A4His was utilized as the template, and each reaction contained the appropriate sense and antisense primers (Figure 2). Mutants S119F/W, I120F/W, A305F/W,

F108W:	GTCTTCACAAACCGGAGGCCC**TGG**GGTCCAGTGGGATTT
S119F (sense):	GAAAAGTGCAATA**TTC**ATAGCTGAGGATGAAGAATGG
S119F (antisense):	CTCAGCTAT**GAA**TATTGCACTTTTCATAAATCCCACTGG
S119W (sense):	GAAAAGTGCCATA**TGG**ATAGCTGAGGATGAAGAATGG
S119W (antisense):	CTCAGCTAT**CCA**TAGGCACTTTTCATAAATCCCACTGG
I120F (sense):	GAAAAGTGCGATATC**TTC**GCTGAGGATG
I120F (antisense):	CATCCTCAGC**GAA**AGATATCGCACTTTTC
I120W (sense):	GTGCCATCAGC**TGG**GCTGAGGATG
I120W (antisense):	CCATTC**TTC**ATCCTCAGC**CCA**GCTGATGGCAC
L210W:	GCGGGATCCAAAAAATCAAATCTTAA**CCA**CTTCTTGGTG
F213W:	GCGGGATCCAAAAAATC**CCA**TCTTAAAAGC
F215W (sense):	CTTTTAAGATTTGAT**TGG**TTAGATCCATTCTTT
F215W (antisense):	AAATCTTAAAAGCTTCTTTTGGTG
I238W:	CTTGAAGTATTAAA**TGG**TGTGTGTTTCCAAGA
I301F/W:	ATCTGGAGCTCGTGGCCCAATCAATT**TKS**TTTATTTTTGC
A305F/W (sense):	CTTTATTTTT**TKS**GGCTATGAAACC
A305F/W (antisense):	AAAAATAAAGATAATTGATTGGG
Y307W (sense):	ATCTTTATTTTTGCTGGC**TGG**GAAACCACGAGC
Y307W (antisense):	AGCAAAAATAAAGATAATTGATTG
T309F/W (sense):	GCTGGCTATGAA**TKS**ACGAGCAGTG
T309F/W (antisense):	CATAGCCAGCAAAAATAAAGATAATTG
I369F/W:	ATGGTGGTTAACGAAACGCTCAGATTATTCCCA**TKS**GCTATGAGA
A370F/W:	ATGGTGGTTAACGAAACGCTCAGATTATTCCCAATT**TKS**ATGAGACTTG
L373F/W:	ATTCCCAATTGCTATGAGA**TKS**GAGAGGGTCTG
L479W (sense):	TGAAATTAAGC**TGG**GGAGGAC**TT**C
L479W (antisense):	GGTTGAAGAAGTCCTCCCCAGCTTAATTTC

FIGURE 2: Primers used for amplification of 3A4 cDNA single mutants. The mutated nucleotides are shown in boldface type. The unique restriction enzyme sites for subcloning are underlined. In the sequences listed above, K represents a mixture of G and T, and the letter S represents a mixture of G and C. These abbreviations follow standard nomenclature.

and L479W were prepared by the overlap PCR extension method (*37*). Plasmid pSE3A4His or pKK3A4His was used as the template. In two separate reactions, the mutagenic sense primers (Figure 2) and downstream vector primer or the mutagenic antisense primers (Figure 2) and upstream vector primer were utilized. Subsequently, the PCR-amplified fragments served as the templates to amplify full-length coding regions with two vector primers. The full-length mutated fragments were cloned directly into pCRII (A305F/W and L479W) or digested with the appropriate restriction enzymes, purified with GeneClean, and ligated into pSE3-A4His that was digested with the same restriction enzymes and purified (S119F/W and I120F/W). The fragments cloned into pCRII were also digested with unique restriction enzymes and subcloned into digested and purified pSE3A4His or pKK3A4His.

Mutants F108W and I238W were constructed in a two-step PCR protocol as previously described (*28*). Each mutagenic primer (Figure 2) was utilized in an amplification reaction with a downstream vector-specific primer. The resulting product was utilized as a primer in a second amplification with an upstream vector-specific primer. The fragment of desired length was digested with unique restriction endonucleases flanking the mutation of interest and subcloned into pSE3A4His that had been digested with the same enzymes and purified. The construction of mutants L210F, F304W, and L479F was described earlier (*19*, *33*, *38*).

Expression and Purification of Mutants. Growth and induction of *Escherichia coli* containing the mutant plasmids were conducted as previously described (*28*). Cells from 250 mL of culture were harvested at 72 h postinduction, washed in 10 mL of buffer A [100 mM MOPS (pH 8.0), 10% glycerol], and resuspended in 10 mL of the same buffer. Each sample was sonicated and centrifuged as previously described (*39*). The pellets were resuspended in 3.75 mL of buffer A, followed by the addition of 0.5% CHAPS and 0.5 M KCl. The samples were slowly stirred on ice for 2 h before centrifugation at 100000*g* at 4 °C for 30 min. The supernatant was removed to a new tube and frozen at −80 °C until being loaded onto a 1 mL talon metal affinity column that had been pre-equilibrated with buffer A plus 0.5% CHAPS and 0.5 M KCl. The protein sample was loaded, and the column was subsequently washed with 10 bed volumes of buffer A, 10 bed volumes of buffer A plus 10 mM imidazole, and 10 bed volumes of buffer A plus 20 mM imidazole. P450 was eluted in buffer A plus 200 mM imidazole. The fractions containing P450 were pooled and dialyzed against two 1 L changes of MOPS buffer [100 mM MOPS (pH 7.3), 10% glycerol, 0.2 mM dithiothreitol, 1.0 mM EDTA]. The P450 content was determined by reduced carbon monoxide difference spectra in the presence of 1% Triton X-100 added to the protein sample before dilution with microsome solubilization buffer [100 mM potassium phosphate (pH 7.3), 20% glycerol, 0.5% sodium cholate, 0.4% Renex, and 1.0 mM EDTA]. Protein purity was analyzed on an 8.5% SDS−polyacrylamide gel. Total protein content in each sample was determined with the BCA Protein Assay kit, and the specific P450 content was determined from the reduced carbon monoxide difference spectrum.

Steroid Hydroxylation Assays. Purified P450 was reconstituted as described previously (*19*) in mixtures (10 μL) containing 0.4% CHAPS and 0.1 mg mL^{-1} DOPC and P450, *E. coli*-expressed rat NADPH−P450 reductase (*29*), and rat cytochrome b_5 in a molar ratio of 1:4:2. Assay mixtures (100 μL) contained 50 mM HEPES (pH 7.6), 15 mM $MgCl_2$, 0.1 mM EDTA, and [^{14}C]progesterone or [^{14}C]testosterone (concentrations of substrate varied and are indicated for each assay in the Results section) in the presence or absence of 25 μM ANF. The reactions contained a final concentration of 2% methanol (v/v) and 0.04% CHAPS. The reactions were started by the addition of 1 mM NADPH and carried out for 5 min at 37 °C before being stopped by the addition of 50 μL of tetrahydrofuran. Metabolites were resolved by thin-layer chromatography, visualized by autoradiography, and quantitated as described previously (*28*).

In kinetic analyses, varying concentrations of steroid were added to the reactions. All other conditions remained the same. Data analysis was performed with Sigma Plot (Jandel Scientific, San Rafael, CA) for values calculated with the Michaelis−Menten equation $v = V_{max}S\,(K_m + S)^{-1}$ and the Hill equation $v = (V_{max}S^n)\,(S_{50}{}^n + S^n)^{-1}$ *(6)*.

ANF Oxidation Assays. Purified 3A4 enzyme (10 pmol) was reconstituted in the presence of 0.4% CHAPS, 0.1 mg mL^{-1} DOPC, 40 pmol of rat NADPH−P450 reductase, and 20 pmol of cytochrome b_5 in 20 μL for 10 min at room temperature. Assay mixtures contained 50 mM HEPES (pH 7.6), 15 mM $MgCl_2$, 0.1 mM EDTA, and 25 μM ANF (unless otherwise indicated). Each 200 μL reaction contained a final concentration of 2% methanol (v/v) and 0.04% CHAPS. The reactions were started by the addition of 1 mM NADPH. After incubation at 37 °C for 10 min, narigenin, used as an internal standard, was added at a final concentration of 2.5 μM, and the reactions were quenched with 500

μL of methylene chloride. The samples were vortexed for 1 min and centrifuged at low speed for 5 min. The combined organic layers from three extractions were transferred to an Eppendorf tube and dried under vacuum. When progesterone was added to the reactions, it was desiccated prior to resuspension in an ANF/methanol solution to maintain the final methanol concentration of 2%. Metabolites were separated with an Alltech Ultrasphere C18 3 μm column (7 $\times$ 53 mm) in 70% methanol at 0.6 mL min^{-1} and detected at 280 nm. The HPLC system consisted of two Beckman 110 solvent delivery modules, a Beckman 421A system controller (Beckman, Berkeley, CA), a Spectroflow 757 UV-absorbance detector (Kratos Analytical, Ramsey, NJ), and a Spectra-Physics SP4270 integrator (Spectra-Physics, Piscataway, NJ). Product formation was quantified by comparison of the peak area to the peak area of substrate, assuming the same extinction coefficient.

7-BFC Debenzylation Assays. Reconstitutions contained purified 3A4 enzyme (5 pmol), 20 pmol of rat NADPH−P450 reductase, 10 pmol of cytochrome b_5, 0.4% CHAPS, and 0.1 mg mL^{-1} DOPC. The mixture was preincubated for 10 min at room temperature. Varying concentrations of 7-BFC were added to the reaction in 50 mM HEPES (pH 7.6), 15 mM $MgCl_2$, and 1.0 mM EDTA. The protein−substrate mixture was further incubated for 5 min at room temperature, and the reaction was initiated by the addition of 1 mM NADPH. The total reaction volume was 100 μL and contained a final methanol concentration of 2% (v/v). After 10 min of incubation at 37 °C the reaction was stopped by the addition of 50 μL of 20% trichloroacetic acid. The mixture was centrifuged at 3000 rpm for 3 min, and 50 μL of the solution was diluted in 2 mL of 100 mM Tris-HCl, pH 9.0. Product formation was measured in a Hitachi F-2000 fluorescence spectrophotometer (Hitachi, San Jose, CA) at an excitation wavelength of 409 nm and emission at 530 nm with a bandwidth of 20 nm at both wavelengths. A blank was run for each sample, and the final activity was calculated by comparison to a standard curve for 7-HFC. The formation of 7-HFC by CYP3A4 was linear over an incubation period of 20 min, and an incubation time of 10 min was employed in subsequent experiments.

RESULTS

Protein Expression, Purification, and Initial Characterization. In this study 23 new Phe or Trp mutants of CYP3A4 were generated and expressed in *E. coli*. Of these, only L373W did not produce any significant heme protein as determined by reduced carbon monoxide difference spectra. The remaining mutants, however, produced P450 levels from 30% up to 100% of wild-type CYP3A4 expression (100−300 nmol L^{-1}) (data not shown). Protein yields upon purification varied from under 15% up to 50%, and the specific contents ranged from 3 to 13 nmol of P450 (mg of total protein)$^{-1}$ (data not shown). Most of the mutants were expressed and purified multiple times. In initial functional characterization with progesterone, testosterone, ANF, and 7-BFC there was no indication that the specific content of a sample affected its activity or metabolite profile. In addition, it was observed that when the initial amino acid residue was other than phenylalanine, substitution with phenylalanine generally resulted in higher activity than with tryptophan.

Steroid Hydroxylation Assays. CYP3A4 and the panel of 25 mutants were analyzed for progesterone (150 μM) and testosterone (250 μM) hydroxylase activity at a single steroid concentration (Figure 3A,B). These assays showed that the mutants could be divided into three groups. The first group, including L210F/W, F213W, F215W, I238W, and I301W, displayed metabolite profiles and overall activities similar to wild-type CYP3A4. The second group, consisting of S119W, A305F/W, T309F/W, I369F/W, and A370F/W, displayed less than one-third of 6β- or total hydroxylase activity toward one or both steroids. The third group consisting of F108W, S119F, I120F/W, I301F, F304W, Y307W, I369F, L373F, and L479F/W showed a >2-fold change in the product ratios from one or both of the steroid hydroxylation assays. In most instances, the positions where Trp or Phe substitutions caused significant alterations of steroid hydroxylation rates or product ratios were the same sites noted in previous studies in which substitutions were of smaller or similar size (*28*−*33*, *38*).

Effect of ANF on Progesterone Hydroxylation by CYP3A4 Mutants. Mutants that displayed significant steroid hydroxylase activity were then tested for stimulation by the effector ANF. In the presence of ANF (25 μM) F108W, S119F, I120W, L210F, F213W, I301F/W, and L373F exhibited diminished stimulation of 6β-OH progesterone formation when compared with CYP3A4 (Table 1). The near wild-type levels of steroid hydroxylation, largely unaltered metabolite profiles, and diminished stimulation in the presence of ANF displayed by L210F, F213W, and I301F suggested a possible role for these sites in cooperativity. Thus, kinetic analysis of progesterone 6β-hydroxylation was performed on these mutants. Plots of these data were hyperbolic in the absence and presence of ANF (25 μM) and confirmed decreased stimulation by the effector over a wide range of substrate concentrations (Figure 4). The kinetic behavior of these mutants is similar to that displayed by CYP3A4 mutant L211F/D214E (*12*). Analysis of residues Leu-211 and Asp-214 indicated their involvement in homotropic and heterotropic cooperativity, and the above data suggest a similar role for Leu-210, Phe-213, and Ile-301 in this process.

ANF Oxidation Assays. Previously, our group found that CYP3A4 displayed cooperative binding of ANF in the absence of NADPH−cytochrome P450 reductase or cytochrome b_5 (*19*). Hosea et al. also reported that the production of ANF 5,6-oxide by CYP3A4 fit best to the Hill equation (*20*). In contrast, Shou et al. have suggested that ANF binds at a single site, whether acting as a substrate or effector, indicated by a K_m value for ANF oxidation similar to the affinity of ANF as an activator of CYP3A4 (*18*, *22*). Therefore, we conducted kinetic analysis of ANF oxidation by our own preparations of CYP3A4 wild type. Data from these assays fit well to the Hill equation ($S_{50} = 14 \pm 1$ μM, $V_{max} = 12 \pm 1$ nmol min^{-1} nmol^{-1}, $n = 2.5 \pm 0.4$) (Figure 5). In the presence of 25 μM progesterone, there was only a slight increase noted in the S_{50} value ($S_{50} = 19 \pm 4$ μM, $V_{max} = 12 \pm 2$ nmol min^{-1} nmol^{-1}, $n = 2.1 \pm 0.7$). However, when the results of several kinetic experiments were compared, the presence of progesterone (25 μM) resulted in the stimulation of ANF 5,6-oxide formation at low concentrations (up to 5 μM) of ANF (Figure 5). Analysis of similar experiments utilizing 25 μM [^{14}C]progesterone verified that

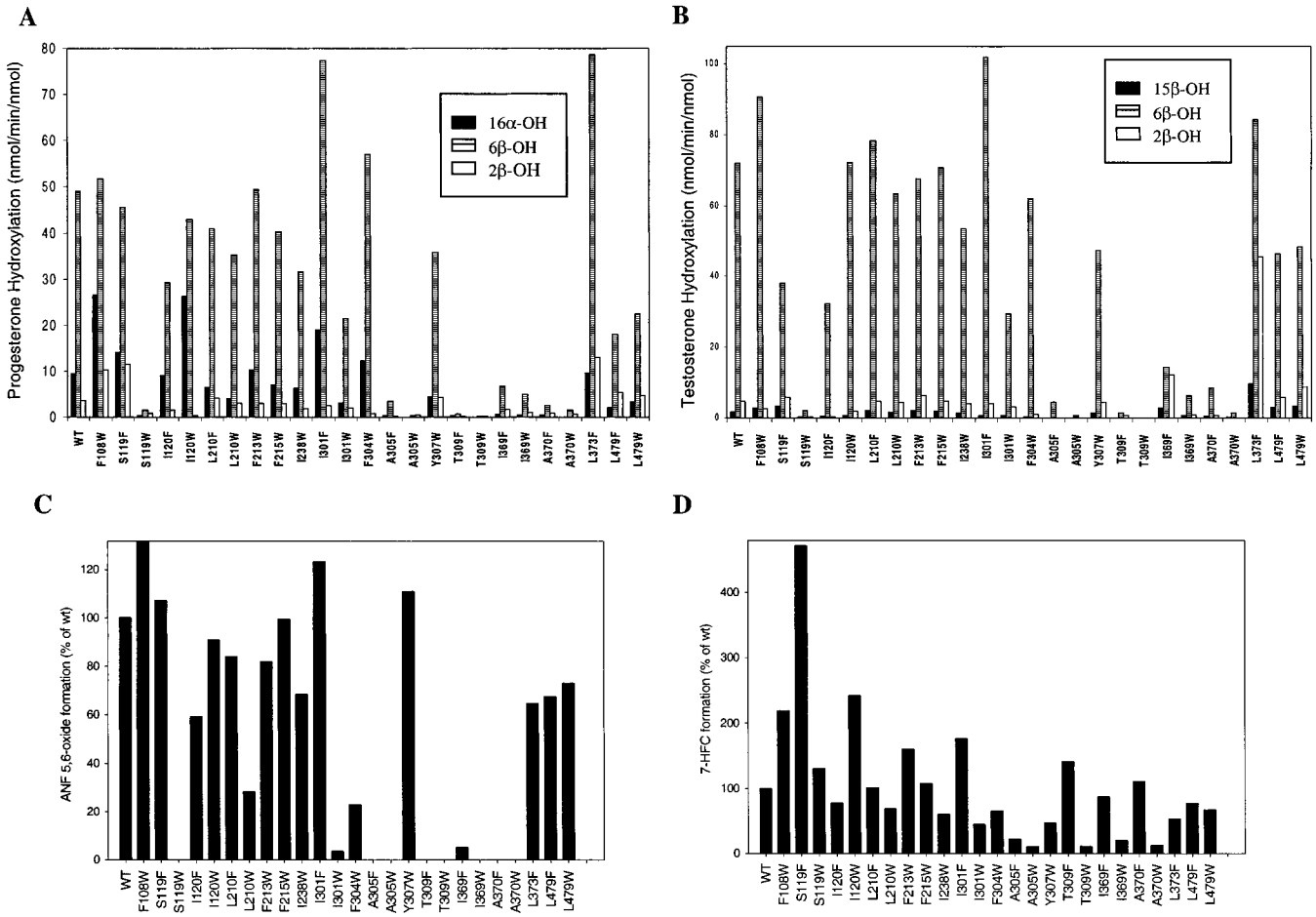

FIGURE 3: Functional assays of CYP3A4 wild type and 25 mutants. (A) Progesterone (150 μM) and (B) testosterone (250 μM) metabolite profiles of CYP3A4 and mutants. (C) Production of ANF 5,6-oxide in assays containing 25 μM ANF and (D) 7-BFC (100 μM) debenzylation by CYP3A4 and a panel of mutants. The activities in (C) and (D) are expressed as percentages of CYP3A4 activity [11.2 nmol of ANF 5,6-oxide min^{-1} (nmol of ANF)$^{-1}$ and 4.4 nmol of 7-HFC min^{-1} (nmol of 7-BFC)$^{-1}$]. All assays were performed as described in Experimental Procedures, and the bars represent the average of values obtained from duplicate determinations.

Table 1: Effect of 25 μM ANF on the Hydroxylation of Progesterone by CYP3A4 and a Panel of Mutants

	methanol			ANF		
sample[a]	16α-OH[b]	6β-OH	2β-OH	16α-OH	6β-OH	2β-OH
CYP3A4	1.7	12.1	0.8	5.9 (3.6)[c]	27.8 (2.3)	3.1 (4.1)
F108W	8.3	20.4	8.1	7.5 (0.9)	26.5 (1.3)	4.8 (0.6)
S119F	2.7	10.3	3.2	4.3 (1.6)	14.4 (1.4)	5.1 (1.6)
I120F	1.6	6.1	<0.1	4.5 (2.8)	22.6 (3.7)	<0.1 (ND)
I120W	9.2	17.4	0.1	10.1 (1.1)	26.0 (1.5)	0.9 (11.1)
L210F	1.8	16.3	1.5	4.0 (2.2)	26.1 (1.6)	3.2 (2.2)
L210W	0.7	9.2	0.9	2.2 (3.0)	24.7 (2.7)	2.5 (2.8)
F213W	2.7	15.8	0.9	4.5 (1.8)	22.2 (1.4)	1.9 (2.1)
F215W	1.4	11.2	1.2	5.8 (4.1)	24.7 (2.2)	3.3 (2.9)
I301F	5.1	27.5	0.5	10.7 (2.1)	30.2 (1.1)	1.5 (3.1)
I301W	1.1	10.4	1.31	1.1 (1.0)	8.0 (0.7)	2.0 (1.5)
L373F	3.2	25.2	3.0	7.3 (2.3)	30.3 (1.2)	8.0 (2.7)
L479F	0.8	8.1	3.0	2.7 (3.3)	18.5 (2.3)	4.9 (1.6)
L479W	1.1	7.4	2.5	2.6 (2.3)	15.5 (2.1)	3.5 (1.4)

[a] In this set of experiments, 3 pmol of P450 per reaction was used. [b] Rates are expressed as nmol of product min^{-1} (nmol of P450)$^{-1}$ and are the average of duplicate determinations. The concentration of progesterone was 25 μM. [c] The numbers in parentheses refer to fold stimulation.

significant stimulation of 6β-OH progesterone formation was observed at all concentrations of ANF from 2.5 to 50 μM (data not shown).

The formation of ANF 5,6-oxide by CYP3A4 and 25 mutants was then measured (Figure 3C). The 25 mutants tested include the 22 newly constructed mutants that expressed efficiently and three additional mutants that were constructed for previous studies (L210F, F304W, and L479F) (*19*, *33*, *38*). Four mutants (L210W, I301W, F304W, and I369F) displayed rates of product formation that were at least 3-fold lower than CYP3A4. Furthermore, eight mutants (S119W, A305F/W, T309F/W, I369W, and A370F/W) did not produce any significant amount of ANF 5,6-oxide. Additional ANF metabolites were not detected for CYP3A4 or any mutant tested in this study.

Correlational Analysis. To assess the relationship between the role of ANF as a substrate and as an effector, the fold stimulation of 6β-OH progesterone production for 12 mutants was compared to the formation of ANF 5,6-oxide expressed as a percentage of CYP3A4 activity (Figure 6). In this correlation, only those mutants that generated at least 10% of CYP3A4 rates of ANF oxidation were included. Using linear regression of the data points, the r^2 value was 0.35, with a negative slope, suggesting only a small but inverse association between ANF as an activator and ANF as a substrate.

7-BFC Debenzylation Kinetics. The utility of 7-BFC as a marker fluorometric substrate for high-throughput screening

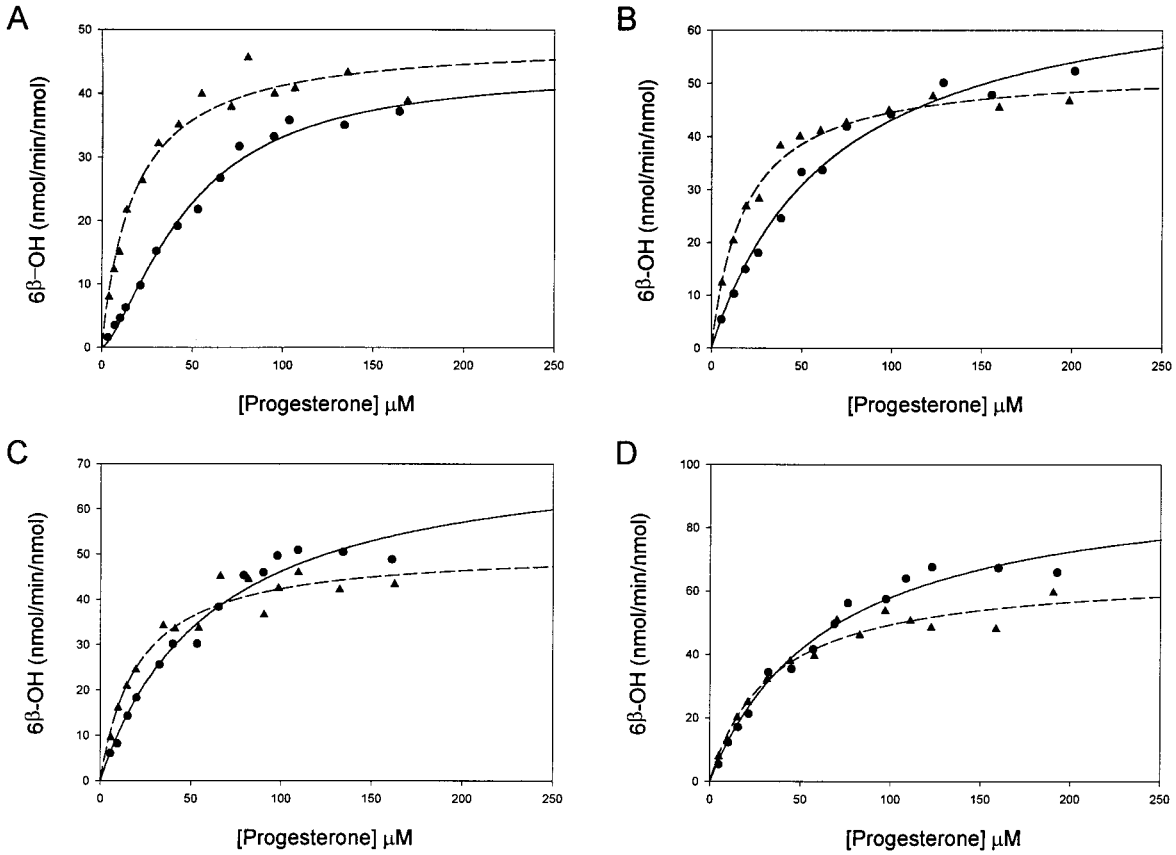

FIGURE 4: Kinetic analysis of progesterone 6β-hydroxylation by CYP3A4 and mutants L210F, F213W, and I301F: (●) absence of ANF; (▲) presence of ANF (25 μM). The graph contains data averaged from duplicate determinations. Data for CYP3A4 in the absence of ANF were analyzed with the Hill equation. All other results were analyzed with the Michaelis−Menten equation as described in Experimental Procedures. Panels: (A) CYP3A4; (B) L210F; (C) F213W; (D) I301F.

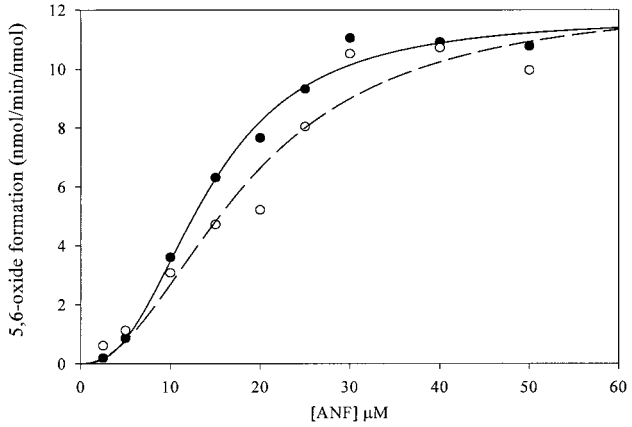

FIGURE 5: Kinetic analysis of ANF 5,6-oxide formation: (●) absence of progesterone; (○) presence of 25 μM progesterone. Data were analyzed with the Hill equation as described in Experimental Procedures to create the ideal curves shown. The graph contains data from duplicate determinations.

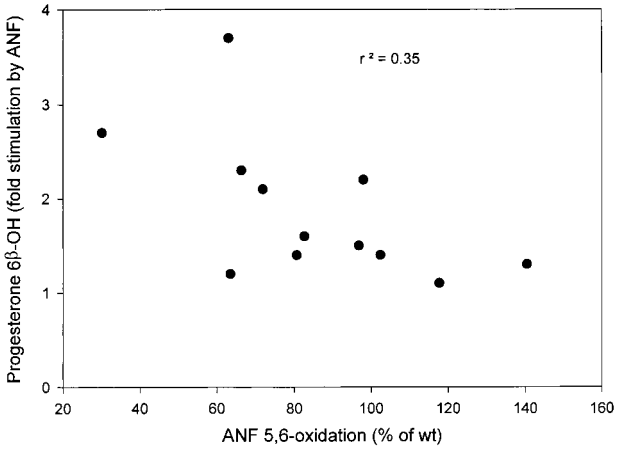

FIGURE 6: Correlation analysis of ANF 5,6-oxide formation versus stimulation of 6β-OH progesterone production by ANF. The graph was generated with Sigma Plot, and the r^2 value was determined from linear regression. Each (●) represents one protein: F108W, S119F, I120F/W, L210F/W, F213W, F215W, I301F, L373F, L479F/W. Only the mutants in this study that displayed over 10% of wild-type CYP3A4 ANF 5,6-oxide production were included.

of CYP3A4 activity and inhibition has been demonstrated (*40*), and in this study 7-BFC was assessed as an active site probe. Initially, a kinetic analysis of 7-BFC debenzylation by CYP3A4 and the double mutant L211F/D214E (*12*) was performed in the absence and presence of ANF (25 μM) (Figure 7A) to compare with previous steroid hydroxylation results. The data for CYP3A4 fit best to the Hill equation, and the plot was sigmoidal ($S_{50} = 31 \pm 9$ μM, $V_{max} = 10 \pm 2$ nmol min^{-1} nmol^{-1}, $n = 1.6 \pm 0.3$) (Figure 7A). In three separate assays, the n value was found to be between 1.5 and 1.7 (data not shown). In the presence of ANF the plot became hyperbolic ($K_m = 31 \pm 7$ μM, $V_{max} = 19 \pm 2$ nmol min^{-1} nmol^{-1}). Our studies of steroid hydroxylation by CYP3A4 and a number of mutants indicate that ANF decreases the S_{50} value without significant change in the V_{max} (*12*, *19*, *28*−*30*). As Figure 7 illustrates, the effect of ANF (25 μM) on 7-BFC debenzylation kinetics is very different and reveals an increase in the V_{max} value. The kinetic

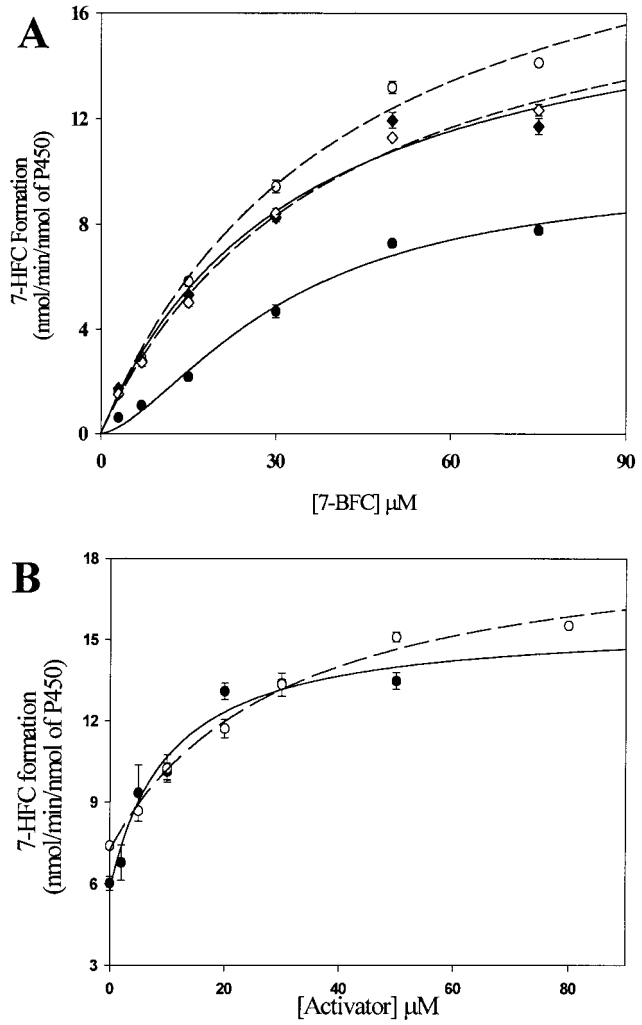

FIGURE 7: Analysis of 7-BFC debenzylation. (A) Kinetic assay of 7-BFC debenzylation by CYP3A4 and L211F/D214E: (●) CYP3A4; (◆) L211F/D214E. Open symbols represent the values obtained in the presence of 25 μM ANF. The data for CYP3A4 in the absence of ANF were analyzed with the Hill equation. All other data were analyzed with the Michaelis−Menten equation as described in Experimental Procedures to create the ideal curves shown. The graph contains data from duplicate determinations and is representative of three independent experiments conducted with CYP3A4 and two experiments with L211F/D214E. (B) Effect of progesterone and ANF on 7-BFC debenzylation by CYP3A4 wild type. Varying amounts of progesterone (○) or ANF (●) were included in assays containing 50 μM 7-BFC. The equation $V = V_0 + V_{max}[E](K_E + [E])^{-1}$ was utilized to analyze the data where V, V_0, and V_{max} represent the oxidation rate at effector [E] concentration, the oxidation rate in the absence of effector, and the maximum rate, respectively. The graph contains data from duplicate determinations and is representative of four independent experiments.

parameters of 7-BFC debenzylation by L211F/D214E were also determined (Figure 7A). As previously found for testosterone hydroxylation *(12)*, the plot of 7-BFC debenzylation by L211F/D214E was hyperbolic in the absence of ANF ($K_m = 26 \pm 7$ μM, $V_{max} = 16 \pm 2$ nmol min^{-1} nmol^{-1}). The addition of ANF (25 μM) had very little effect on the kinetic parameters ($K_m = 35 \pm 4$ μM, $V_{max} = 18 \pm 1$ nmol min^{-1} nmol^{-1}). Likewise, progesterone (25 μM) did not stimulate 7-BFC debenzylation by L211F/D214E (data not shown).

The finding that ANF alters the V_{max} value but not the S_{50} for CYP3A4-catalyzed 7-BFC debenzylation facilitated determination of the affinity for the effectors progesterone and ANF. 7-BFC oxidation assays were thus performed at a single concentration of substrate (50 μM) in the presence of varying amounts of ANF or progesterone (Figure 7B). The binding constants, K_E, for ANF and progesterone were found to be 10 ± 4 and 30 ± 7 μM, respectively. The 3-fold higher affinity of ANF is consistent with the ability of progesterone to stimulate ANF oxidation only at low concentrations of ANF. To test the validity of this approach, an experiment was conducted in which both progesterone (5, 15, 30, 50 μM) and 7-BFC (10, 20, 30, 50 μM) concentrations were varied (data not shown). The K_E for progesterone was found to be 25 ± 7 μM, in excellent agreement with the value obtained at 50 μM 7-BFC. Furthermore, there was no inhibition of 7-BFC oxidation by progesterone under any of the conditions (data not shown). The corresponding lack of inhibition of progesterone 6β-hydroxylation by 7-BFC was further demonstrated in assays containing 25 μM steroid and 7-BFC at varying concentrations up to 50 μM (Table 2). With testosterone as a substrate for wild-type CYP3A4, 7-BFC caused up to 30% stimulation of 6β-hydroxylation (Table 2). However, with L211F/D214E, no inhibition or stimulation of testosterone 6β-hydroxylation was noted at concentrations of 7-BFC up to 100 μM (data not shown).

Table 2: CYP3A4 Steroid Hydroxylation at Varying 7-BFC Concentrations

7-BFC (μM)	6β-OH progesterone[a]	6β-OH testosterone[a]
0	19.0	10.3
5	17.7	11.7
10	19.5	12.8
25	20.0	13.2
50	18.8	12.2

[a] The values are expressed as nmol of product min^{-1} (nmol of P450)$^{-1}$ and are derived from assays performed in duplicate. The substrate concentration was 25 μM for each steroid.

CYP3A4 and a panel of 25 mutants were then assayed for 7-BFC debenzylase activity at a single concentration of substrate (100 μM) (Figure 3D). A variety of P450 to rat NADPH−cytochrome P450 reductase to cytochrome b_5 molar ratios were tested to determine optimal reconstitution conditions. The 1:4:2 molar ratio described in Experimental Procedures for steroid hydroxylation was found to be optimal for 7-BFC debenzylation (data not shown). Mutants F108W, S119F, and I120W exhibited activities at least 2-fold higher than 3A4 (Figure 3D). In addition, it is intriguing that a number of the mutants that displayed very little progesterone or testosterone hydroxylase activity (S119W, A305W, T309F/W, I369F/W, and A370F) were able to catalyze significant levels of 7-HFC formation. In fact, S119W, T309F, and A370F displayed rates of 7-HFC production similar to that observed for CYP3A4, although they displayed <5% of CYP3A4 rates of 6β-OH progesterone or 6β-OH testosterone formation.

Correlational Analysis of Substrate Oxidation by CYP3A4 Mutants. The results obtained from the comparison of ANF as an effector versus ANF as a substrate suggested the utility of using the panel of mutants in correlational analyses of the separate enzymatic activities. Such analyses might help to define the relative positions of individual substrate binding. Correlations between individual activities for the 25 mutants analyzed in this study were assessed in sets of two, from

Table 3: Correlation between Activities of CYP3A4 Mutants

	6β-OH progesterone	7-HFC	ANF 5,6-oxide
6β-OH testosterone	0.86[a,b]	0.11	0.69
ANF 5,6-oxide	0.59	0.30	
7-HFC	0.15		

[a] The correlations are expressed as r^2 values calculated in Sigma Plot using the linear regression function. [b] Each r^2 value represents data from the panel of 25 mutants.

which r^2 values were calculated (Table 3). From these analyses, the suspected colocalization of the 6β-progesterone and 6β-testosterone binding orientations was confirmed ($r^2 = 0.86$). This was suggested from competition studies between these two substrates in a previous study (*12*). The poor correlation between oxidation of ANF and 7-BFC ($r^2 = 0.30$) was consistent with the lack of inhibition by ANF of 7-BFC debenzylation (Figure 7B). Likewise, correlations between progesterone and 7-BFC ($r^2 = 0.15$) and testosterone and 7-BFC ($r^2 = 0.11$) were low. The low r^2 value between 7-BFC and progesterone or testosterone is consistent with the lack of mutual inhibition between 7-BFC and the steroid substrates. The somewhat higher r^2 value found between ANF and progesterone or testosterone may indicate a partial overlap of these binding positions. This complex interaction between ANF and steroids is also shown in the effect of progesterone on ANF oxidation (Figure 5), in which progesterone appears to stimulate ANF oxidation at low ANF concentrations but may inhibit as the substrate concentration increases.

DISCUSSION

CYP3A4 plays a major role in xenobiotic metabolism in human liver, and a mechanistic understanding of the inhibition and activation of the enzyme is especially relevant to the study of drug−drug interactions. The past half-decade has seen an increase in studies seeking to better define the interaction of multiple substrates with CYP3A4 and elucidate (1) how one compound can stimulate its own oxidation or that of another compound and (2) how in some cases two compounds can be oxidized at the same time without demonstrating competition (*6*, *11*, *12*, *18*−*2*6, *41*). Three different approaches have been utilized in these studies.

Several groups have analyzed CYP3A4 cooperativity with mathematical models applied to large sets of steady-state kinetic data. Shou et al. first suggested that two compounds, such as ANF and phenanthrene, can simultaneously occupy the CYP3A4 binding pocket (*18*). Ueng and co-workers subsequently analyzed the effect of reconstitution conditions on the activity of recombinant CYP3A4, the steady-state kinetics with a number of substrates in the absence and presence of ANF, and the oxidation of ANF in the presence of aflatoxin B_1 (*6*). The authors found that several of the substrates demonstrated homotropic cooperativity and/or stimulation by ANF, and they proposed an allosteric model to explain their data, although the proximity of the putative allosteric site to the catalytic site could not be ascertained. In a later study, kinetic models were utilized to demonstrate that many of the atypical properties that have been described for CYP3A4 and other cytochromes P450, including activation, autoactivation, partial inhibition, and substrate inhibition, could be explained with a two-site model (*22*). However, one unique solution for sigmoidal saturation kinetics could not be determined, and the model described could not distinguish whether each substrate occupied a preferred position. A separate model to explain the sigmoidal kinetic characteristics of diazepam and its derivatives was proposed (*11*). The data and the rate constants derived provided more information about the allosteric nature of CYP3A4, but the approach was still limited by the inability to provide any structural insight. More recently, this group analyzed the interaction between ANF and losartan (*23*). The results suggested that there is a preferred position within the CYP3A4 binding pocket for ANF and that losartan has a preferred location depending on the product formed (sites S1 and S2 in Figure 1A). The ongoing use and development of mathematical models have been useful in explaining much of the atypical kinetic behavior displayed by CYP3A4. However, these models have not been able to provide any clues as to the location of the putative subpockets within the CYP3A4 active site, nor has there been any attempt to use them to explain the interaction of compounds that each show homotropic cooperativity.

Others have used inhibitors to perturb the CYP3A4 active site, characterized the effect on a number of substrate/effector pairs, and classified the substrates on the basis of the results. Kenworthy et al. examined the interaction of 10 probe substrates and found that they could be divided into three groups related to their size or chemical class (*42*). The authors predicted that analysis of CYP3A4 drug−drug interactions might be conducted with CYP3A4 and a single member of each substrate class. A separate study utilized short peptides that interact with the heme iron of P450 through nitrogen ligation, although they are not oxidized (*20*). The effect of these peptides on the binding and oxidation of midazolam, testosterone, and ANF was examined, and the results indicated that both ANF and midazolam bind to two sites in the binding pocket and that three sites probably exist in CYP3A4. However, the authors readily acknowledge that their work did not provide information about the location or juxtaposition of these multiple sites.

Site-directed mutagenesis has become an accepted methodology for probing the active site of cytochromes P450 (reviewed in ref *43*). The lack of a CYP3A4 crystal structure does present the limitation of only having a molecular model of uncertain exactness to analyze mutagenesis results. However, comparison of the crystal structure of CYP2C5 with that of bacterial P450s indicated that most of the secondary structure elements and topological features that define the active site are conserved (*34*). Our laboratory and others have utilized site-directed mutagenesis to identify over a dozen amino acid residues that are important determinants of CYP3A4 substrate specificity (*28*−*33*, *38*, *44*) and that have direct active site counterparts in CYP2C5 (*35*). In addition, site-directed mutagenesis was used to identify three CYP3A4 amino acid residues, Leu-211, Asp-214, and Phe-304, that play significant roles in cooperativity (*12*, *19*). Site-directed mutagenesis is the only approach of those discussed that has provided any data implicating specific CYP3A4 amino acid residues in specific functions.

In the present study, a combination of site-directed mutagenesis and a functional analysis with four substrates was utilized to further probe the active site. This strategy

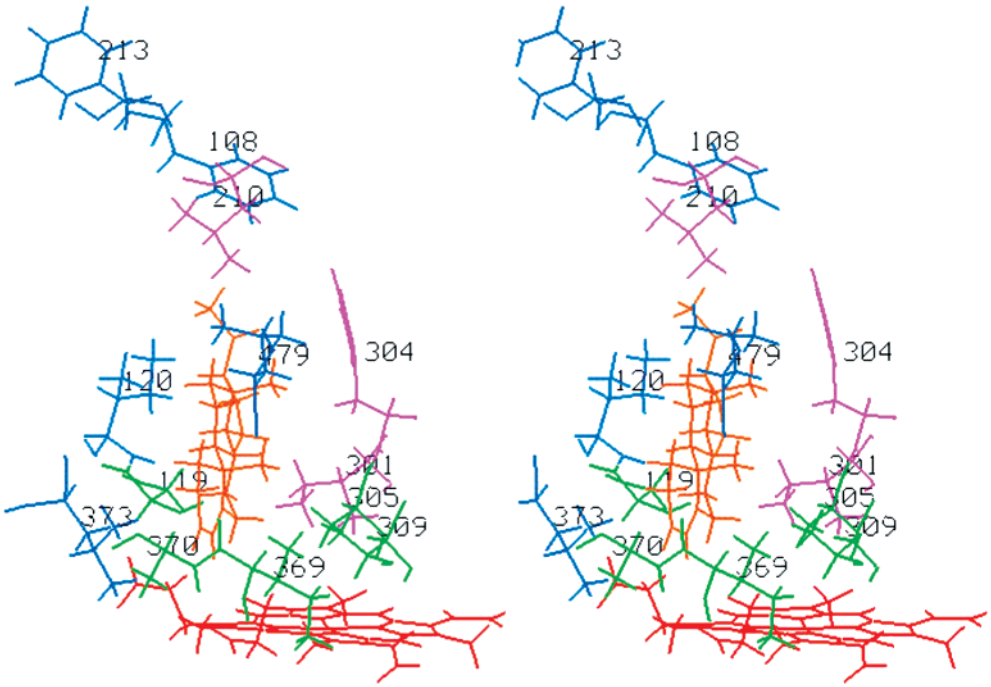

FIGURE 8: Molecular model of CYP3A4. The CYP3A4 structure was refined by realignment of the F- and B′-helices using the homology and biopolymer modules of Insight II (*44*). The heme is shown in red, and a portion of the putative binding pocket is shown in stereoview. The side chains of interest are labeled in black. Progesterone is docked in the 6β-hydroxy orientation and depicted in orange. Amino acid residues were grouped according to the effect of alterations at each site. The side chains of residues Phe-108, Ile-120, Phe-213, Leu-373, and Leu-479 are shown in blue. Mutation at these sites caused less than a 2-fold change in any of the four tested activities. Residues where Trp substitution preferentially decreased ANF oxidation over steroid or 7-BFC oxidation are shown in violet (Leu-210, Ile-301, Phe-304). Those side chains shown in green represent sites where the Phe and/or Trp mutants exhibited decreased steroid and ANF oxidation relative to 7-BFC debenzylation (Ser-119, Ala-305, Thr-309, Ile-369, Ala-370).

provided data on the interaction between separate substrates in the CYP3A4 binding pocket and the role of individual amino acid residues in substrate oxidation and cooperativity. The kinetics of ANF and 7-BFC oxidation by CYP3A4 were analyzed. The effect that steroids, ANF, and 7-BFC have on each other's oxidation by CYP3A4 was examined, and the role that 15 individual amino acid residues play in determining the positioning of one and/or more of these substrates in the CYP3A4 binding pocket was explored. The findings from this study indicate that (1) ANF and 7-BFC oxidation follow sigmoidal kinetics (Figures 5 and 7A), (2) progesterone slightly stimulates ANF oxidation at low substrate concentrations (Figure 5), (3) ANF has a 3-fold higher affinity for the putative effector site than progesterone (Figure 7B), (4) there is only a poor correlation between the oxidation of ANF and stimulation by ANF of progesterone 6β-hydroxylation when comparing 12 of the mutants studied (Figure 6), (5) 7-BFC and progesterone/testosterone do not compete for oxidation by CYP3A4, and (6) correlational analyses using pairwise comparisons of functions for the 25 mutants studied match with predictions about the interaction between the substrates from competitition experiments.

As mentioned in the previous sections, the number of subpockets within the CYP3A4 active site and the positioning of compounds within have not been fully defined, and three possible explanations have been proposed (Figure 1). First, the model depicted in Figure 1B suggests that only one molecule would have access to the reactive oxygen. However, the lack of inhibition observed between a number of substrate pairs cannot be easily explained by the orientation of molecules in model 1B (Figures 4, 5, and 7A). While the recently published structure of $P450_{eryF}$ indicates that this P450 can contain two molecules of androstenedione in a similar orientation (*27*), the situation in CYP3A4 must be more complex, as Hosea et al. also suggested in their recent study (*20*). Figure 1A also depicts only two possible binding positions in CYP3A4 but shows both molecules having access to the reactive oxygen. However, our data in total cannot be fully explained by this model. 7-BFC does not demonstrate competition with testosterone or progesterone for oxidation, and 7-BFC, like progesterone and testosterone, displays homotropic cooperativity. In addition, 7-BFC oxidation and testosterone or progesterone 6β-hydroxylation by the 25 mutants in this study do not show any significant correlation. These data suggest that 7-BFC is preferentially oxidized from a site distinct from progesterone or testosterone and that 7-BFC and the steroids have some affinity for the E site. These data fit well with the three-site model depicted in Figure 1C, although it is possible that the two-site model in Figure 1B could also explain our data if functionally distinct conformers are invoked (*21*). In this case separate conformers that oxidize 7-BFC or progesterone and testosterone exist, and both conformers are able to bind any of the three molecules as effectors.

In a previous study, substitutions at residues Leu-211 and Asp-214 were shown to preferentially decrease the stimulation of progesterone and testosterone 6β-hydroxylation by ANF without altering the metabolite profile in the absence of this effector molecule (*12*). In addition, hyperbolic steady-state kinetics of L211F/D214E-catalyzed steroid hydroxylation were observed in the absence of ANF. In the present study, three mutants, L210F, F213W, and I301F, displayed progesterone and testosterone hydroxylation phenotypes similar to that of L211F/D214E (Figures 3A,B and 4). These

findings suggest that, at least for the interaction between ANF and progesterone in the CYP3A4 active site, residues Leu-210, Phe-213, and Ile-301 are important factors in the action of effector.

One common feature of the two-site (1A) and three-site (1C) models is the hypothesis that at least some CYP3A4 substrates preferentially bind either at S1 or at S2. Although there is some support for distinct sites (*11*, *20*, *23*), there has not been data that can pinpoint their locations. However, our comparison of the residual activity of each mutant toward progesterone, testosterone, ANF, and 7-BFC suggested three phenotypes. First, alterations at several positions did not appear to significantly affect protein function, and the mutants retained over 50% of their ability to oxidize the steroids, ANF, and 7-BFC (Phe-108, Ile-120, Phe-213, Phe-215, Leu-373, and Leu-479) (blue in Figure 8). Second, Trp substitutions at several residues resulted in a preferential loss of ANF oxidation when compared with steroid or 7-BFC oxidation (Leu-210, Ile-301, and Phe-304) (violet in Figure 8). Third, substitutions at several sites caused the loss of steroid hydroxylation and ANF oxidation but did not decrease 7-BFC debenzylation to a similar degree (Ser-119, Ala-305, Thr-309, Ile-369, and Ala-370) (side chains in green in Figure 8). The position of the side chains in each group in Figure 8 suggests the presence of a subpocket that lies close to the heme (green) and a separate subpocket that is more distal (violet). While models 1A and 1C show specific positions for S1 and S2, there are likely areas of crossover, such as residues that affect steroid and ANF oxidation, but others that appear to be more specific for ANF oxidation. This is also illustrated in the analyses that show a high correlation between progesterone and testosterone 6β-hydroxylation, a very low correlation between 7-BFC debenzylation and the other activities, but a midrange r^2 value for ANF oxidation when compared with testosterone or progesterone 6β-hydroxylation (Table 2).

In conclusion, a three-site model has been proposed to account for the data presented in this study, in agreement with a similar model presented recently (*20*). In addition, evidence for preferential substrate binding at distinct locations within the active site was presented. While no single technique has proven perfect for revealing the mechanistic and structural basis of the atypical kinetic behavior of CYP3A4, it is encouraging to find that both site-directed mutagenesis and the use of inhibitors have resulted in the proposal of three-site models. The complexity of CYP3A4 cooperativity suggests that future studies should include mathematical, structural, and functional studies in a more concerted effort.

ACKNOWLEDGMENT

The authors thank Ms. You-Qun He (Department of Pharmacology and Toxicology, University of Texas Medical Branch, Galveston, TX) for providing several of the mutants characterized in this study and Dr. Jill Cupp-Vickery (Department of Chemistry and Biochemistry, California State University, Fullerton, CA) for input and insightful comments.

REFERENCES

1. Evans, W. E., and Relling, M. V. (1999) *Science 286*, 487−491.
2. Li, A. P., Kaminski, D. L., and Rasmussen, A. (1995) *Toxicology 104*, 1−8.
3. Buters, J. T. M., Korzekwa, K. R., Kunze, K. L., Omata, Y., Hardwick, J. P., and Gonzalez, F. J. (1994) *Drug Metab. Dispos. 22*, 688−692.
4. Fuhr, U., Weiss, M., Kroemer, H. K., Neugebauer, G., Rameis, H., Weber, W., and Woodcock, B. G. (1996) *Int. J. Clin. Pharmacol. Ther. 34*, 139−151.
5. Ueng, Y., Shimada, T., Yamazaki, H., and Guengerich, F. P. (1995) *Chem. Res. Toxicol. 8*, 218−225.
6. Ueng, Y. F., Kuwabara, T., Chun, Y. J., and Guengerich, F. P. (1997) *Biochemistry 36*, 370−381.
7. Grant, D. M., Campbell, M. E., Tang, B. K., and Kalow, W. (1987) *Biochem. Pharmacol. 36*, 1251−1260.
8. Kerr, B. M., Thummel, K. E., Wurden, C. J., Klein, S. M., Kroetz, D. L., Gonzalez, F. J., and Levy, R. H. (1994) *Biochem. Pharmacol. 47*, 1969−1979.
9. Schwab, G. E., Raucy, J. L., and Johnson, E. F. (1988) *Mol. Pharmacol. 33*, 493−499.
10. Andersson, T., Miners, J. O., Veronese, M. E., and Birkett, D. J. (1994) *Br. J. Clin. Pharmacol. 38*, 131−137.
11. Shou, M., Mei, Q., Ettore, M. W., Dai, R., Baillie, T. A., and Rushmore, T. H. (1999) *Biochem. J. 340*, 845−853.
12. Harlow, G. R., and Halpert, J. R. (1998) *Proc. Natl. Acad. Sci. U.S.A. 95*, 6636−6641.
13. Huang, M. T., Chang, R. L., Fortner, J. G., and Conney, A. H. (1981) *J. Biol. Chem. 256*, 6829−6836.
14. Lasker, J. M., Huang, M. T., and Conney, A. H. (1984) *J. Pharmacol. Exp. Ther. 277*, 287−291.
15. Lasker, J. M., Huang, M. T., and Conney, A. H. (1982) *Science 216*, 1419−1421.
16. Tang, W., Stearns, R. A., Wang, R. W., Chiu, S.-H. L., and Baillie, T. A. (1999) *Chem. Res. Toxicol. 12*, 192−199.
17. Tang, W., Stearns, R. A., Kwei, G. L., Iliff, S. A., Miller, R. R., Egan, M. A., Yu, N. X., Dean, D. C., Kumar, S., Shou, M., Lin, J. H., and Baillie, T. A. (1999) *J. Pharmacol. Exp. Ther. 291*, 1068−1074.
18. Shou, M., Grogan, J., Mancewica, J. A., Krausz, K. W., Gonzalez, F. J., Gelboin, H. V., and Korzekwa, K. R. (1994) *Biochemistry 33*, 6450−6455.
19. Domanski, T. L., He, Y. A., Harlow, G. R., and Halpert, J. R. (2000) *J. Pharmacol. Exp. Ther. 293*, 585−591.
20. Hosea, N. A., Miller, G. P., and Guengerich, F. P. (2000) *Biochemistry 39*, 5929−5939.
21. Koley, A. P., Buters, J. T. M., Robinson, R. C., Markowitz, A., Friedman, F. K. (1997) *J. Biol. Chem. 272*, 3149−3152.
22. Korzekwa, K. R., Krishnamachary, N., Shou, M., Ogai, A., Parise, R. A., Rettie, A. E., Gonzalez, F. J., and Tracy, T. S. (1998) *Biochemistry 37*, 4137−4147.
23. Shou, M., Dais, R., Cui, D., Korzekwa, K. R., Baillie, T. A., and Rushmore, T. H. (2001) *J. Biol. Chem. 276*, 2256−2262.
24. Wang, R. W., Newton, D. J., Scheri, T. D., and Lu, A. Y. H. (1997) *Drug Metab. Dispos. 25*, 502−507.
25. Wang, R. W., Newton, D. J., Atkins, W. M., and Lu, A. Y. H. (2000) *Drug Metab. Dispos. 28*, 360−366.
26. Kenworthy, K. E., Clarke, S. E., Andrews, J., and Houston, J. B. (1998) in *12th International Symposium on Microsomes and Drug Oxidations*, p 136, Montpellier, France.
27. Cupp-Vickery, J., Anderson, R., and Hatziris, Z. (2000) *Proc. Natl. Acad. Sci. U.S.A. 97*, 3050−3055.
28. Domanski, T. L., Liu, J., Harlow, G. R., and Halpert, J. R. (1998) *Arch. Biochem. Biophys. 350*, 223−232.
29. Harlow, G. R., and Halpert, J. R. (1997) *J. Biol. Chem. 272*, 5396−5402.
30. He, Y. A., He, Y. Q., Szklarz, G. D., and Halpert, J. R. (1997) *Biochemistry 36*, 8831−8839.
31. Khan, K. K., and Halpert, J. R. (1999) *Arch. Biochem. Biophys. 373*, 335−345.
32. Roussel, F., Khan, K. K., and Halpert, J. R. (1999) *Arch. Biochem. Biophys. 374*, 269−278.
33. Wang, H., Dick, R., Yin, H., Licad-Coles, E., Kroetz, D. L., Szklarz, G. D., Harlow, G. R., Halpert, J. R., and Correia, M. A. (1998) *Biochemistry 37*, 12536−12545.

34. Williams, P. A., Cosme, J., Sridhar, V., Johnson, E. F., and McRee, D. E. (2000) *Mol. Cell 5*, 121−131.
35. Domanski, T. L., and Halpert, J. R. (2001) *Curr. Drug Metab.* (in press).
36. Domanski, T. L., Schultz, K. M., Roussel, F., Stevens, J. C., and Halpert, J. R. (1999) *J. Pharmacol. Exp. Ther. 290*, 1141−1147.
37. Stemmer, W. P., Morris, S. K., and Wilson, B. S. (1993) *BioTechniques 14*, 256−265.
38. Stevens, J. C., Domanski, T. L., Harlow, G. R., White, R. B., Orton, E., and Halpert, J. R. (1999) *J. Pharmacol. Exp. Ther. 290*, 594−602.
39. John, G. H., Hasler, J. A., He, Y., and Halpert, J. R. (1994) *Arch. Biochem. Biophys. 314*, 367−375.
40. Stresser, D. M., Blanchard, A. P., Turner, S. D., Erve, J. C., Dandeneau, A. A., Miller, V. P., and Crespi, C. L. (2000) *Drug Metab. Dispos. 28*, 1440−1448.
41. Ekins, S., Ring, B. J., Binkley, S. N., Hall, S. D., and Wrighton, S. A. (1998) *Int. J. Clin. Pharmacol. Ther. 36*, 642−651.
42. Kenworthy, K. E., Bloomer, J. C., Clarke, S. E., and Houston, J. B. (1999) *Br. J. Clin. Pharmacol. 48*, 716−727.
43. von Wachenfeldt, C., and Johnson, E. F. (1995) in *Cytochrome P450* (Ortiz de Montellano, P. R., Ed.) pp 183−223, Plenum Press, New York.
44. Xue, L., Wang, H., Szklarz, G. D., Domanski, T. L., Halpert, J. R., and Correia, M. A. (2001) *Chem. Res. Toxicol*. (in press).

BI010758A